Atmos. Chem. Phys., 22, 10139–10153, 2022
https://doi.org/10.5194/acp-22-10139-2022

Atmospheric Chemistry and Physics
Open Access
EGU

Measurement report: Large contribution of biomass burning and aqueous-phase processes to the wintertime secondary organic aerosol formation in Xi'an, Northwest China

Jing Duan[1], Ru-Jin Huang[1,2,3,4], Yifang Gu[1,4], Chunshui Lin[1], Haobin Zhong[1,4], Wei Xu[1], Quan Liu[5], Yan You[6], Jurgita Ovadnevaite[7], Darius Ceburnis[7], Thorsten Hoffmann[8], and Colin O'Dowd[7]

[1]State Key Laboratory of Loess and Quaternary Geology (SKLLQG), CAS Center for Excellence in Quaternary Science and Global Change, Institute of Earth Environment, Chinese Academy of Sciences, 710061 Xi'an, China
[2]Open Studio for Oceanic-Continental Climate and Environment Changes, Pilot National Laboratory for Marine Science and Technology (Qingdao), 266000 Qingdao, China
[3]Institute of Global Environmental Change, Xi'an Jiaotong University, 710049 Xi'an, China
[4]University of Chinese Academy of Sciences, 100049 Beijing, China
[5]State Key Laboratory of Severe Weather & Key Laboratory of Atmospheric Chemistry of CMA, Chinese Academy of Meteorological Sciences, 100081 Beijing, China
[6]National Observation and Research Station of Coastal Ecological Environments in Macao, Macao Environmental Research Institute, Macau University of Science and Technology, 999078 Macao SAR, China
[7]School of Physics and Centre for Climate and Air Pollution Studies, Ryan Institute, National University of Ireland Galway, H91CF50 Galway, Ireland
[8]Department of Chemistry, Johannes Gutenberg University Mainz, 55128 Mainz, Germany

Correspondence: Ru-Jin Huang (rujin.huang@ieecas.cn) and Quan Liu (liuq@cma.gov.cn)

Received: 21 February 2022 – Discussion started: 3 March 2022
Revised: 11 July 2022 – Accepted: 13 July 2022 – Published: 9 August 2022

Abstract. Secondary organic aerosol (SOA) plays an important role in particulate air pollution, but its formation mechanism is still not fully understood. The chemical composition of non-refractory particulate matter with a diameter $\leq 2.5\,\mu m$ (NR-$PM_{2.5}$), OA sources, and SOA formation mechanisms were investigated in urban Xi'an during winter 2018. The fractional contribution of SOA to total OA mass (58 %) was larger than primary OA (POA, 42 %). Biomass-burning-influenced oxygenated OA (OOA-BB) was resolved in urban Xi'an and was formed from the photochemical oxidation and aging of biomass burning OA (BBOA). The formation of OOA-BB was more favorable on days with a larger OA fraction and higher BBOA concentration. In comparison, the aqueous-phase processed oxygenated OA (aq-OOA) was more dependent on the secondary inorganic aerosol (SIA) content and aerosol liquid water content (ALWC), and it showed a large increase (to 50 % of OA) during SIA-enhanced periods. Further van Krevelen (VK) diagram analysis suggests that the addition of carboxylic acid groups with fragmentation dominated OA aging on reference days, while the increased aq-OOA contributions during SIA-enhanced periods likely reflect OA evolution due to the addition of alcohol or peroxide groups.

Published by Copernicus Publications on behalf of the European Geosciences Union.

1 Introduction

Particulate matter with a diameter $\leq 2.5\,\mu m$ ($PM_{2.5}$) in the atmosphere has become an important environmental problem with respect to climate, visibility, and human health, especially in China due to rapid industrialization, urbanization, and population expansion (Huang et al., 2014; Lelieveld et al., 2015; Peng et al., 2016; An et al., 2019). Most megacities in China have been frequently plagued by severe particulate pollution in recent years, attracting extensive attention and research on the composition characteristics and formation mechanisms of this pollution (Guo et al., 2014; Hu et al., 2013, 2016; Li et al., 2017; Tong et al., 2017; Sun et al., 2016, 2018). Haze pollution occurs more frequently in winter due to unfavorable meteorological conditions as well as a myriad of other variables, such as complex emission sources, pollutant lifetimes, and atmospheric reactions (Sun et al., 2013, 2014; Elser et al., 2016; Hu et al., 2016; An et al., 2019; Kuang et al., 2020).

Fine particulate matter can either be emitted directly from primary sources, which is referred to as primary aerosol, or produced in the atmosphere through gas-to-particle conversion or aging of primary aerosol, which is referred to as secondary aerosol (Jimenez et al., 2009; Liu et al., 2010; Xu et al., 2017). Numerous studies have elucidated the increasing importance of secondary aerosol in haze pollution (Sun et al., 2016; Huang et al., 2014, 2019; An et al., 2019; Duan et al., 2021). However, the formation and evolution of secondary aerosol, especially secondary organic aerosol (SOA), is still not well understood, and this is becoming a critical concern for air pollution research (Gilardoni et al., 2016; Xu et al., 2017; Kuang et al., 2020; Zhang et al., 2021a; Li et al., 2022a; Lv et al., 2022). Deficits in the understanding of variable precursors, complex transformation, and the aging chemistry of SOA lead to insufficient knowledge of its formation as well as uncertainty in model simulations (Shrivastava et al., 2017).

Field studies based on aerosol mass spectrometer (AMS) measurements combined with OA source apportionment techniques (Paatero, 1999; DeCarlo et al., 2006; Canonaco et al., 2013) have been conducted in China to resolve SOA sources and investigate SOA formation and evolution mechanisms (Hu et al., 2013, 2016; Sun et al., 2016; Xu et al., 2017, 2019). Gas-phase photochemical oxidation has been considered as a major pathway of SOA formation in a number of studies, according to the correlation between SOA and odd oxygen, which is defined as O_x ($O_x = O_3 + NO_2$) (Sun et al., 2014; Elser et al., 2016; Hu et al., 2016). However, recent studies have also revealed the important contribution of aqueous-phase chemistry (which is missing in SOA simulation and is difficult to identify) to SOA formation (Guo et al., 2014; Sun et al., 2016; Xu et al., 2017, 2019; Huang et al., 2020; Li et al., 2021). For example, Sun et al. (2016) resolved an aqueous-phase processed oxygenated SOA (aq-OOA), which significantly affected the OA oxidation state under high-RH conditions (>50 %). The results from Wang et al. (2017) and Xu et al. (2017) indicated that aqueous-phase chemistry played a dominant role in the formation of more highly oxidized oxygenated OA (MO-OOA). Kuang et al. (2020) further resolved the contribution of photochemical aqueous-phase chemistry in wintertime haze pollution, finding that it induced the rapid formation of SOA in the daytime.

As the largest city in the Guanzhong Basin, one of the top three regions in China's air cleaning campaign, Xi'an has suffered serious particulate pollution in recent years due to rapid urbanization; however, research on aerosol composition and SOA formation mechanisms in the region are still limited (Elser et al., 2016; Zhong et al., 2020; Duan et al., 2021). Elser et al. (2016) analyzed the chemical composition and OA sources of $PM_{2.5}$ during the heavy-pollution period of 2013 in Xi'an using a high-resolution AMS (HR-AMS); they found that the contribution of SOA increased during extreme haze events, but the SOA formation mechanism and OA oxidation state during haze pollution were not well analyzed. As multiple control measures have been implemented in Xi'an, such as the "13th Five-Year Comprehensive Energy Conservation and Emission Reduction Plan" (Wan et al., 2022) and motor vehicle restrictions, it is expected that the aerosol composition and sources have varied largely in recent years, although direct elucidation and characterization are lacking. Recent studies have shown that biomass burning and secondary formation dominated the OA concentration in Xi'an and that these sources contributed >50 % of the total OA in both autumn and winter (Zhong et al., 2020). In addition, Xiao et al. (2020) reported that biomass burning sources, especially residential biofuel, can contribute to increased urban NH_3 emissions. Several studies have also indicated that biomass burning is an important source of light-absorbing components in Xi'an (Zhang et al., 2020; Yuan et al., 2021; Zhang et al., 2021b; Li et al., 2022b). Wu et al. (2018) revealed that simultaneously elevated RH and anthropogenic secondary inorganic aerosol (SIA) resulted in an abundant aerosol liquid water content (ALWC), which can further facilitate the formation of heavy haze. Zhong et al. (2020) indicated that OOA formation was most likely dominated by aqueous-phase processes when O_x was <35 ppb in Xi'an in autumn and winter, and Duan et al. (2021) found that persistently high RH and ALWC were the driving factors of aq-OOA formation in Xi'an in summer and that the increasing trend in aq-OOA was very similar to that of nitrate. These studies indicate the importance of biomass burning as well as aqueous-phase reactions in Xi'an, which need further elucidation.

In this study, the $PM_{2.5}$ composition was measured in Xi'an during the residential heating season of 2018 using a soot particle long-time-of-flight AMS (SP-LToF-AMS). The chemical composition and OA sources were analyzed and compared with those resolved in Elser et al. (2016) in order to elucidate the aerosol variation in recent years due to emission controls. Meanwhile, the SOA formation mechanisms

and SOA contribution to haze events were investigated and compared with those in the summer of 2019 (Duan et al., 2021). The main objectives of our study were to investigate the dominant variables mediating aq-OOA formation and to quantify the changing contributions of SOA between seasons and years in Xi'an.

2 Experimental section

2.1 Sampling

The winter campaign was conducted from 4 December 2018 to 15 March 2019 at the campus of the Institute of Earth Environment, Chinese Academy of Sciences (34°23′ N, 108°89′ E; 12 m a.g.l., meters above ground level) in downtown Xi'an, which is surrounded by residential, commercial, and traffic areas (Duan et al., 2021).

A SP-LToF-AMS (Aerodyne Research Inc.) was deployed for the online characterization of $PM_{2.5}$ with a time resolution of 1 min. The detailed instrument description can be found in Onasch et al. (2012), and a similar operation was conducted to that outlined in Duan et al. (2021). The contribution of black carbon (BC) was not considered, and only the non-refractory particulate matter with a diameter $\leq 2.5\,\mu m$ (NR-$PM_{2.5}$) composition, including organics (OA), nitrate (NO_3^-), sulfate (SO_4^{2-}), ammonium (NH_4^+), and chloride (Cl^-), was analyzed. Briefly, ambient air was sampled into the room at a flow rate of $5\,L\,min^{-1}$. After being dried by a Nafion dryer (MD-700-24S, Perma Pure, Inc.), the ambient aerosol was focused into a particle beam using a $PM_{2.5}$ aerodynamic lens; it was subsequently subsampled into the SP-LToF-AMS at a flow rate of $\sim 0.1\,L\,min^{-1}$. The particle beam was vaporized upon impacting the heated tungsten surface ($\sim 600°$) and was ionized by electron ionization (70 eV) to produce positive fragments, which were detected and analyzed by the LToF mass spectrometer. The ionization efficiency (IE) and relative ionization efficiency (RIE) calibrations were conducted during the campaign using 350 nm ammonium nitrate (NH_4NO_3) and ammonium sulfate ($(NH_4)_2SO_4$) particles (Jimenez et al., 2003). Meanwhile, gases including CO, NO_2, O_3, and SO_2 were measured using a Thermo Scientific Model 48i carbon monoxide analyzer, a Thermo Scientific Model 42i NO–NO_2–NO_x analyzer, a Thermo Scientific Model 49i ozone analyzer, and an ecotech EC9850 sulfur dioxide analyzer, respectively. The meteorological parameters, including relative humidity (RH), temperature, wind speed, and wind direction, were measured by an automatic weather station (for RH and temperature; MAWS201, Vaisala, Vantaa, Finland) and a wind sensor (for wind speed and direction; QMW101-M2, Vaisala, Vantaa, Finland).

2.2 Data analysis

The SQUIRREL and PIKA software packages, coded in Igor Pro (WaveMetrics), were used to analyze the SP-LToF-AMS data (https://cires1.colorado.edu/jimenez-group/ToFAMSResources/ToFSoftware/index.html, last access: 10 July 2022). Standard RIEs of 1.4, 1.1, and 1.3 were used for organics, nitrate, and chloride, respectively, whereas experimentally determined RIEs of 3.7 and 1.3 were used for ammonium and sulfate, respectively. Meanwhile, the composition-dependent collection efficiency (CDCE) was used to calibrate and compensate for incomplete detection due to particle bounce (Middlebrook et al., 2012). Note that the RH was not considered in the CDCE calculations, as a Nafion dryer was used and the RH effects on collection efficiency were much reduced. The elemental ratios, including the oxygen-to-carbon (O/C) and hydrogen-to-carbon (H/C) ratios, and the organic mass-to-organic carbon (OM/OC) ratio were also analyzed for the high-resolution OA mass spectra based on the improved ambient (I-A) method (Canagaratna et al., 2015). Meanwhile, the data and error matrices of high-resolution OA mass spectra for m/z 12–120 were preprocessed, and OA source apportionment was performed using positive matrix factorization (PMF) and multilinear engine (ME-2) in Igor Pro (Paatero, 1999), as conducted in Duan et al. (2021).

In addition, the ALWC was also calculated based on the ISORROPIA II model using inorganic aerosol composition (NH_4^+, SO_4^{2-}, NO_3^-, and Cl^-) combined with ambient temperature and RH as input data (Fountoukis and Nenes, 2007). The simulation was run in "metastable" mode, in which all components are assumed to be deliquescent and no solid matter is present. The thermodynamic equilibrium and phase state of those inorganic species were then simulated, and the ALWC was resolved.

3 Results and discussion

3.1 Overview of NR-$PM_{2.5}$ composition and OA sources in Xi'an in winter

The NR-$PM_{2.5}$ concentration varied from 5.9 to $205.6\,\mu g\,m^{-3}$ with an average value of $68.0 \pm 42.8\,\mu g\,m^{-3}$ in Xi'an during the winter of 2018 (see Fig. 1 and Table S1 in the Supplement; note that all of the values given in the following are the arithmetic means and standard deviations of the per-minute samples over the campaign or specified subperiod). This average concentration was higher than that measured in Xi'an in the summer of 2019 ($22.3 \pm 11.7\,\mu g\,m^{-3}$; Duan et al., 2021), due to the higher source emissions in winter than in summer, which has also been observed in other cities (Sun et al., 2015; Xu et al., 2014, 2016). Meanwhile, the average NR-$PM_{2.5}$ concentration observed in our study was much lower than those observed in Xi'an in the winter of 2013 ($125.0 \pm 99.0\,\mu g\,m^{-3}$

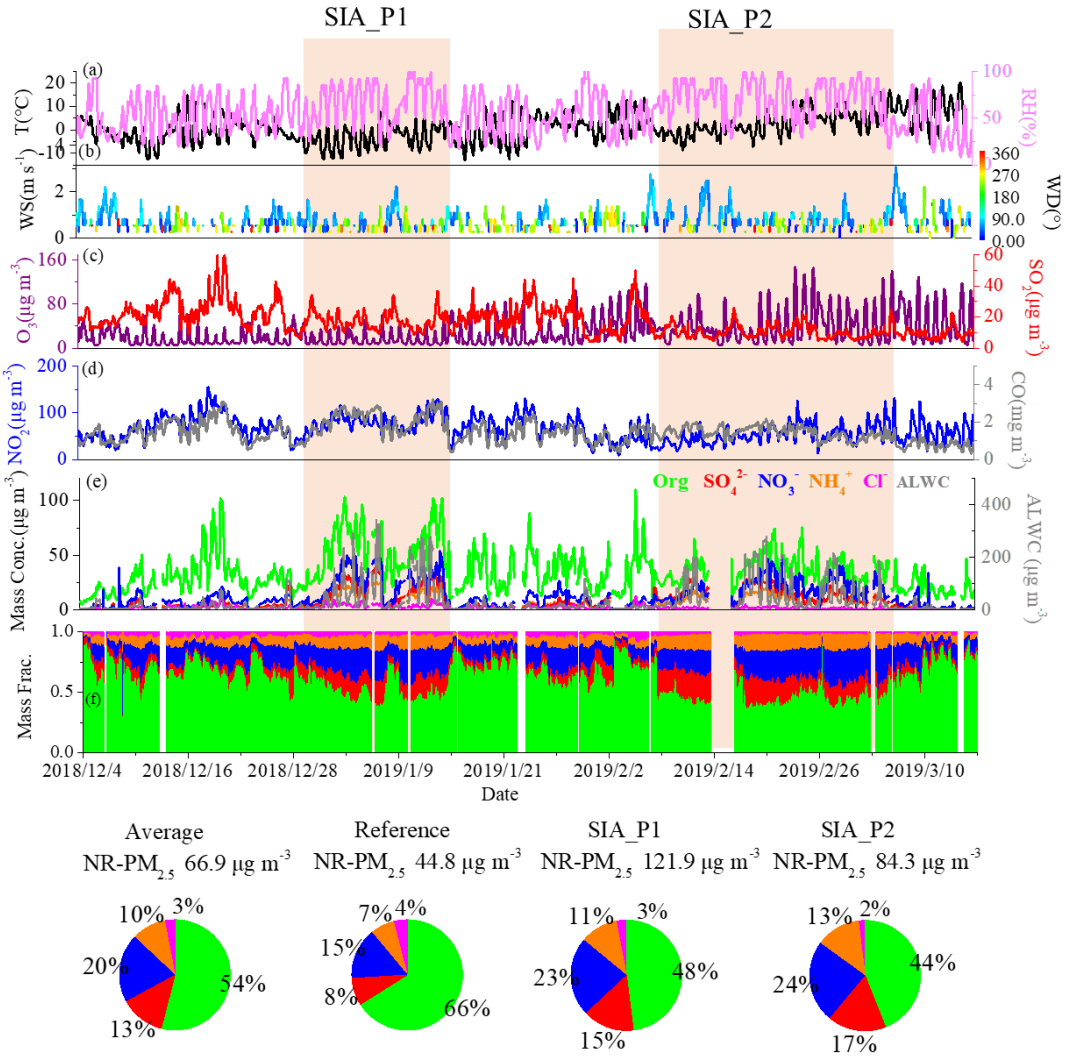

Figure 1. Time series of **(a, b)** meteorological parameters (relative humidity – RH, temperature – T, wind speed – WS, and wind direction – WD), **(c, d)** gases (SO_2, O_3, NO_2, and CO), **(e)** the aerosol liquid water content (ALWC), and **(f)** the NR-$PM_{2.5}$ composition in Xi'an in the winter of 2018. The average composition of NR-$PM_{2.5}$ for the entire winter campaign as well as for reference days and SIA-enhanced periods (SIA_P1 and SIA_P2) are also shown using pie charts.

during reference days and $498.0 \pm 146.0\,\mu g\,m^{-3}$ during haze days) (Elser et al., 2016), pointing to improved air quality. However, haze events with NR-$PM_{2.5}$ concentrations higher than $100\,\mu g\,m^{-3}$ were still frequently observed during the campaign, indicating some overlooked pollution sources or atmospheric formation pathways which require further attention. As for the chemical composition, OA constituted a dominant fraction (54 %) of the total NR-$PM_{2.5}$ mass, although this was lower than the contribution observed in Xi'an in summer (63 %). Nitrate contributed 20 % to the total NR-$PM_{2.5}$ mass, followed by sulfate (13 %), ammonium (10 %), and chloride (3 %). The higher contribution of nitrate than sulfate was the inverse of the situation observed in summer, during which time there was a higher contribution from sulfate (17 %) than nitrate (12 %), suggesting the increased formation and contribution of nitrate in winter pollution, likely due to the much lower temperature in winter which facilitated the partitioning of nitrate into the particle phase (Duan et al., 2021). Meanwhile, the contribution of nitrate in our campaign was also higher than that observed in Xi'an during the winter of 2013 (by 13 % during haze days and by 10 % during reference days) (Elser et al., 2016), suggesting the increasing importance of nitrate pollution compared with sulfate pollution in recent years, consistent with the interannual evolution trend of nitrate observed in Beijing (Xu et al, 2019).

Six OA sources were resolved, including a hydrocarbon-like OA (HOA), a cooking OA (COA), a biomass burning OA (BBOA), a coal combustion OA (CCOA), a biomass-burning-influenced oxygenated OA (OOA-BB), and an

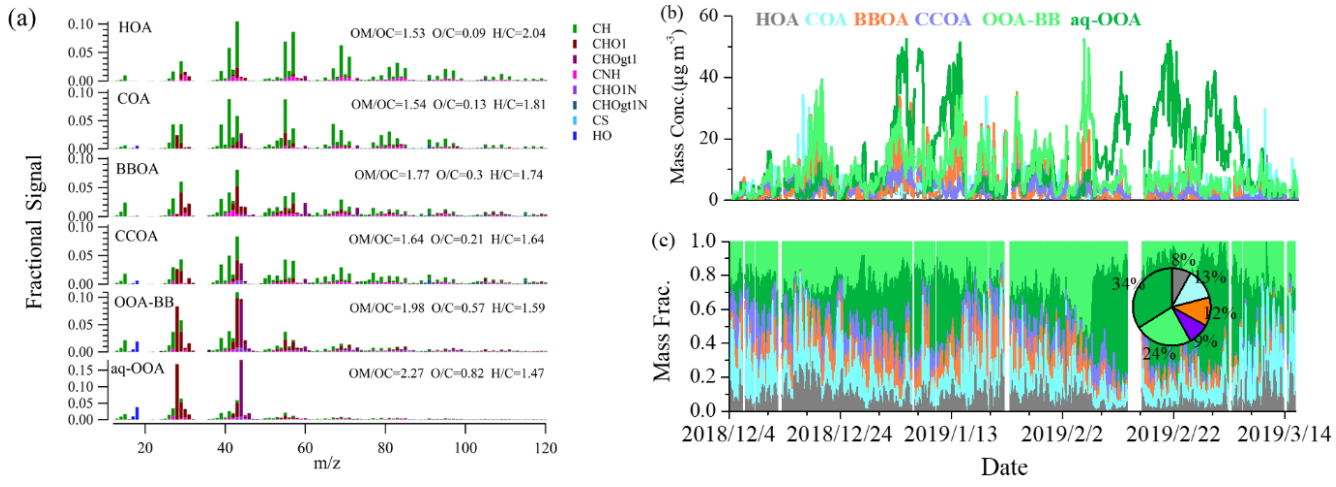

Figure 2. Panel **(a)** presents the mass spectra of OA sources, and panels **(b)** and **(c)** show the respective time series of the concentration and fraction of each OA source in total OA mass during the winter campaign. The average composition of OA sources for the entire observation is also shown as pie chart in the inset in panel **(c)**.

aqueous-phase processed oxygenated OA (aq-OOA) (Fig. 2; OA source apportionment is detailed in the Supplement). Primary OA (POA), including HOA, COA, CCOA, and BBOA, contributed 42 % in total to OA mass. HOA contributed 8 % ($3.0 \pm 3.9\,\mu g\,m^{-3}$) to the total OA mass (Fig. 2). This contribution was lower than that observed in winter 2013 (18 %, $23.0 \pm 27.0\,\mu g\,m^{-3}$, on reference days and 16 %, $49.0 \pm 41.0\,\mu g\,m^{-3}$, on extreme haze days) (Elser et al., 2016), which may be related to the better traffic control in urban Xi'an in recent years. COA contributed 13 % ($4.8 \pm 4.2\,\mu g\,m^{-3}$) to total OA on average, which was higher than that observed in Xi'an during winter 2013 (9 %, $15.8 \pm 8.7\,\mu g\,m^{-3}$, on reference days and 4 %, $33.0 \pm 16.0\,\mu g\,m^{-3}$, on extreme haze days) (Elser, et al., 2016). CCOA contributed 9 % ($3.2 \pm 2.5\,\mu g\,m^{-3}$) to total OA on average during this winter campaign, consistent with the values observed in the winter of 2013 (14 %, $5.7 \pm 4.1\,\mu g\,m^{-3}$, on reference days and 6 %, $7.7 \pm 8.0\,\mu g\,m^{-3}$, on extreme haze days) (Elser et al., 2016). In comparison, BBOA was a more significant contributor than CCOA, accounting for 12 % ($4.3 \pm 5.9\,\mu g\,m^{-3}$) of total OA mass on average. However, this contribution was much lower than that observed in Xi'an in the winter of 2013 (42 %, $22.0 \pm 20.0\,\mu g\,m^{-3}$, on reference days and 43 %, $67.0 \pm 40.0\,\mu g\,m^{-3}$, on extreme haze days) (Elser et al., 2016), suggesting the reduction of BBOA emissions in Xi'an and its surrounding areas in recent years. SOA contributed a higher fraction (58 %, $21.8 \pm 7.4\,\mu g\,m^{-3}$) than POA to total OA, with OOA-BB and aq-OOA accounting for 24 % and 34 % of OA mass, respectively. The contribution of SOA was much higher than that observed in Xi'an in the winter of 2013 (16 %, $5.4 \pm 8.9\,\mu g\,m^{-3}$, on reference days and 31 %, $47.0 \pm 12.0\,\mu g\,m^{-3}$, on haze days) (Elser et al., 2016).

A continuous and large increase in SIA (nitrate, sulfate, and ammonium) was observed during two periods: from 30 December 2018 at 00:00 to 15 January 2019 at 06:00 LT (SIA-enhanced period 1 – SIA_P1) and from 7 February 2019 at 00:00 to 4 March 2019 at 23:00 LT (SIA-enhanced period 2 – SIA_P2). Other periods are defined as reference days. During the reference days, OA contributed a major fraction of 66 % to total NR-$PM_{2.5}$ mass, which was even higher than the contribution in Xi'an during the summer of 2019 (63 %) (Duan et al., 2021). In comparison, the 66 % contribution of OA on reference days decreased to 52 % during SIA_P1 and to 44 % during SIA_P2, and the contribution of SIA increased from 30 % on reference days to 45 % during SIA_P1 and to 53 % during SIA_P2. Meanwhile, the SIA-enhanced periods were also related to a higher $PM_{2.5}$ concentration, which increased from $44.1 \pm 25.5\,\mu g\,m^{-3}$ during reference days to $131.0 \pm 49.6\,\mu g\,m^{-3}$ during SIA_P1 and to $84.9 \pm 30.7\,\mu g\,m^{-3}$ during SIA_P2, suggesting an important contribution of SIA to the formation of haze pollution in Xi'an in winter (Zhong et al., 2020; Zhang et al., 2021b). The major difference between SIA-enhanced periods and reference days was the very frequent occurrence of a higher relative humidity (RH>60 %) and ALWC concentration (ALWC>$10\,\mu g\,m^{-3}$) during SIA_P1 and SIA_P2 compared with reference days (Fig. S1 in the Supplement). This indicated the more frequent occurrence of liquid-phase conditions during SIA-enhanced periods compared with reference days. According to previous studies, high RH and liquid-phase reactions play important roles in the formation of secondary inorganic aerosol, such as sulfate and nitrate (Sun et al., 2016; Wu et al., 2018). Thus, high RH and liquid-phase conditions may drive the large production of SIA in Xi'an in winter (Xu et al., 2019; Duan et al., 2021).

During our measurement, the concentration of ammonium increased from $3.3 \pm 2.2\,\mu g\,m^{-3}$ during reference days to $13.3 \pm 6.5\,\mu g\,m^{-3}$ during SIA_P1 and to $10.8 \pm 4.6\,\mu g\,m^{-3}$

during SIA_P2, consistent with the variation trends in sulfate and nitrate (sulfate increased from $3.5 \pm 2.8\,\mu g\,m^{-3}$ during reference days to $18.4 \pm 10.2\,\mu g\,m^{-3}$ during SIA_P1 and to $14.7 \pm 7.2\,\mu g\,m^{-3}$ during SIA_P2, whereas nitrate increased from $6.8 \pm 4.9\,\mu g\,m^{-3}$ during reference days to $27.4 \pm 13.4\,\mu g\,m^{-3}$ during SIA_P1 and to $19.9 \pm 9.3\,\mu g\,m^{-3}$ during SIA_P2). The equivalent molar concentration of ammonium correlated tightly with that of the total of sulfate and nitrate with a slope of ≈ 1 during all three periods (reference days, SIA_P1, and SIA_P2), suggesting that ammonium was mainly neutralized by sulfate and nitrate in Xi'an in winter, both on reference days and during SIA-enhanced periods (Fig. S2).

Specifically, in order to further analyze the relative importance of sulfate and nitrate in haze pollution, the increased respective contributions of sulfate and nitrate during SIA periods compared with reference days (the "increase ratios", IRs) were calculated following the equations below:

$$IR_{sulfate} = f_{sulfate,SIA} / f_{sulfate,reference};$$
$$IR_{nitrate} = f_{nitrate,SIA} / f_{nitrate,reference}.$$

Here, $IR_{sulfate}$ and $IR_{nitrate}$ refer to the respective increase ratios of the sulfate contribution and the nitrate contribution from reference days to SIA periods; $f_{sulfate,SIA}$ and $f_{nitrate,SIA}$ refer to the respective mass fractions of sulfate and nitrate in total $PM_{2.5}$ mass during SIA periods (including SIA_P1 and SIA_P2); and $f_{sulfate,reference}$ and $f_{nitrate,reference}$ refer to the respective mass fractions of sulfate and nitrate in total $PM_{2.5}$ mass during reference days.

The $IR_{sulfate}$ from reference days to SIA_P1 (1.8) and to SIA_P2 (2.1) was higher than the $IR_{nitrate}$ values (1.4 from reference days to SIA_P1 and 1.5 from reference days to SIA_P2). Meanwhile, the average mass ratio of NO_3^-/SO_4^{2-} (Sun et al., 2016) decreased from 1.9 during reference days to 1.5 during SIA_P1 and to 1.4 during SIA_P2. These trends suggest that the increase in the sulfate contribution during haze pollution was much more obvious than that of the nitrate contribution in Xi'an in winter, although the absolute concentration of nitrate was higher than sulfate, both on reference days and during SIA periods. NO_3^-/SO_4^{2-} showed an evident decrease as a function of RH at higher NR-$PM_{2.5}$ loading ($>50\,\mu g\,m^{-3}$) (Fig. S1). Consistently, although both the sulfur oxidation ratio (SOR – defined as $n[SO_4^{2-}]/(n[SO_4^{2-}] + n[SO_2])$, where n indicates the molar concentration of SO_4^{2-} or SO_2; Ji et al., 2018; Chang et al., 2020) and the nitrogen oxidation ratio (NOR – defined as $n[NO_3^-]/(n[NO_3^-] + n[NO_2])$, where n indicates the molar concentration of NO_3^- or NO_2; Ji et al., 2018; Chang et al., 2020) increased with RH, SOR increased from 0.10–0.20 at RH<40 % to 0.33–0.63 at RH>60 %, which was more efficient than the increase in NOR (from 0.07–0.10 at RH<40 % to 0.18–0.30 at RH>60 %) (Fig. S3). These results suggest that a high RH is more favorable in sulfate formation than in nitrate formation, especially under haze pollution conditions in Xi'an in winter.

As discussed above, the SIA-enhanced periods were usually related to haze pollution with higher NR-$PM_{2.5}$ mass. The OA composition between reference days and SIA-enhanced periods was further compared in order to better understand the OA evolution during haze pollution in Xi'an (Fig. S9). From reference days to SIA_P1, the total mass of OA increased from 28.7 ± 16.4 to $68.0 \pm 20.7\,\mu g\,m^{-3}$ (Table S1). Both POA and SOA concentrations increased, with aq-OOA increasing the most, from 4.9 ± 3.7 to $26.2 \pm 14.6\,\mu g\,m^{-3}$. As a result, the O/C ratio of the bulk OA increased from 0.41 ± 0.10 on reference days to 0.52 ± 0.10 during SIA_P1, suggesting an enhanced OA oxidation state during SIA_P1. In comparison, the total mass of OA ($37.7 \pm 11.7\,\mu g\,m^{-3}$) during SIA_P2 was higher than that on reference days, whereas it was lower than that during SIA_P1. The POA and OOA-BB mass concentrations were lower than those both on reference days and during SIA_P1, and the increase in the total OA mass from reference days to SIA_P2 was dominantly ascribed to the dramatic increase in aq-OOA from 4.9 ± 3.7 to $22.7 \pm 10.7\,\mu g\,m^{-3}$, similar to that from reference days to SIA_P1. As a result, the O/C ratio of total OA during SIA_P2 was further enhanced to 0.67 ± 0.11, which was much higher than those on reference days and during SIA_P1. This suggests a much higher OA oxidation state during SIA_P2 than on reference days and during SIA_P1.

3.2 OOA-BB dependence on BBOA and photochemical oxidation

We further analyzed the evolution and formation mechanism of OOA-BB, and we found that the time variation in OOA-BB correlated well with that of BBOA ($R^2 = 0.59$) (Fig. S7), with peaks of m/z 60 ($C_2H_4O_2^+$) and m/z 73 ($C_3H_5O_2^+$) in the mass spectrum of OOA-BB (Fig. 2), indicating the possible influence of a BBOA source on the formation of OOA-BB. Note that, although a moderate correlation was observed between the time series of OOA-BB and BBOA, lags and differences between their time series were observed, suggesting atmospheric aging under environmental conditions.

The fragment ions of m/z 60 ($C_2H_4O_2^+$) and m/z 73 ($C_3H_5O_2^+$) generated from the pyrolysis of cellulose, such as levoglucosan and mannosan, were considered to be good tracers of BBOA (Alfarra et al., 2007; Cubison et al., 2011). Fresh BBOA usually exhibits the highest content of m/z 60 ($C_2H_4O_2^+$) and m/z 73 ($C_3H_5O_2^+$), which will decrease due to oxidation reactions and degradation during atmospheric aging. At the same time, oxygenated fragments such as m/z 44 (CO_2^+) will increase during atmospheric aging (Cubison et al., 2011; Paglione et al., 2020). The correlation and evolution of f_{60} (the fraction of m/z 60 in the total signal of the OA mass spectrum) and f_{44} (the fraction of m/z 44 in the total signal of the OA mass spectrum) are usually used to analyze the influence of BBOA on SOA as well as the evo-

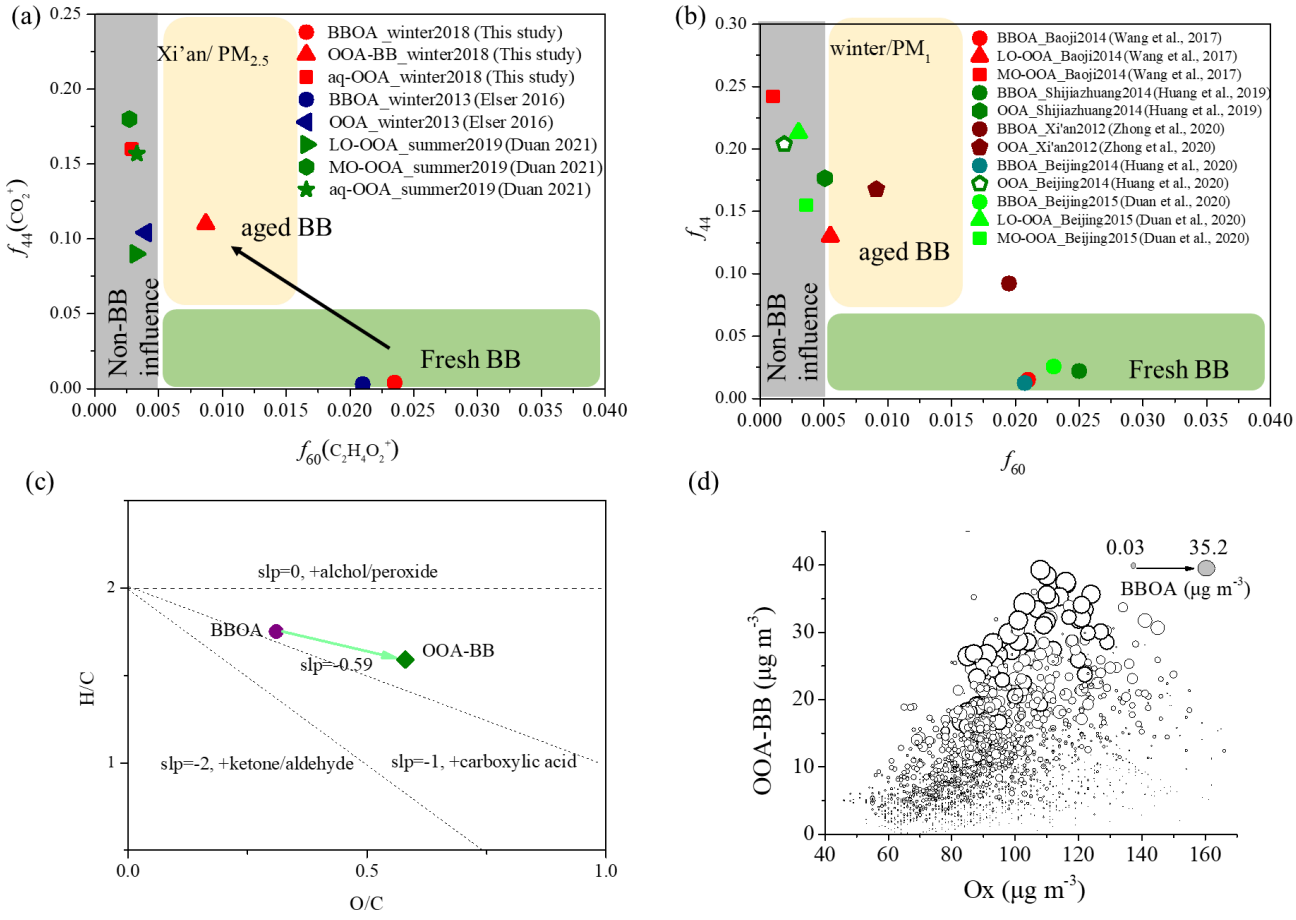

Figure 3. Panel **(a)** presents f_{44} vs. f_{60} for BBOAs and SOAs resolved in OA of $PM_{2.5}$ in Xi'an; panel **(b)** shows f_{44} vs. f_{60} for BBOAs and SOAs resolved in OA of PM_1 in our previous campaigns conducted in Xi'an, Baoji, Shijiazhuang, and Beijing; panel **(c)** gives the van Krevelen (VK) diagram of the BBOA and OOA-BB factors resolved in Xi'an in the winter of 2018; and panel **(d)** shows the effects of the O_x and BBOA concentrations on OOA-BB formation.

lution processes of BBOA and SOA (Cubison et al., 2011). As $PM_{2.5}$ was measured in our campaign, in order to further analyze the influence of BBOA on SOA formation in Xi'an, OA sources in $PM_{2.5}$ (resolved using AMS) were compared. Figure 3a displays f_{44} (f_{CO_2+}) vs. f_{60} ($f_{C_2H_4O_2+}$) plots for BBOA and SOA sources resolved in the winter of 2018 (this campaign), the winter of 2013 (Elser et a., 2016), and the summer of 2019 (Duan et al., 2021). According to Cubison et al. (2011), $f_{60} = 0.003 \pm 0.002$ represents the threshold of BB influence. Therefore, SOA sources with an f_{60} higher than 0.005 suggested the influence of BBOA, whereas f_{60}<0.003 suggested a secondary source with no influence from BBOA. Fresh biomass burning emission sources usually have high f_{60} and low f_{44} values. As shown in Fig. 3, the BBOA factors resolved in the winter of 2018 and 2013 were both located in the fresh-BBOA region, with a higher $f_{C_2H_4O_2+}$ (0.024 and 0.021, respectively, which were both higher than 0.005) and lower f_{CO_2+}, suggesting they were fresh BBOA emissions. OOA-BB (Paglione et al., 2020) resolved in the winter of 2018 was characterized by an $f_{C_2H_4O_2+}$ value of 0.08 and an f_{CO_2+} value of 0.13, located in the BB-influenced region, indicating that the OOA-BB resolved in the winter of 2018 was largely influenced by BBOA emissions. In comparison, the aq-OOA (Sun et al., 2016) resolved in the winter of 2018, the OOA resolved in the winter of 2013, and the three SOA sources (LO-OOA, MO-OOA, and aq-OOA) resolved in the summer of 2019 all showed higher f_{CO_2+} and lower $f_{C_2H_4O_2+}$ (<0.005) values, located in the non-BB-influenced region, suggesting that these SOAs were formed from other processes independent of BBOA sources. In addition, in order to further compare the BBOA influence on SOA among different regions, f_{44} vs. f_{60} values for BBOA and SOA resolved in PM_1-OA from previous studies were also compared (see Fig. 3b; additional data from our previous studies are also shown). In most studies, BBOA is located in the fresh-BBOA region, except for the BBOA resolved in Xi'an in the winter of 2012 (Zhong et al., 2020). Meanwhile, most of the SOAs were located in the non-BB-influenced region, except for the OOA resolved in the winter of 2012 (Zhong et al., 2020) which showed a

higher f_{44} of 0.17 and a higher f_{60} of 0.09 (>0.05). This further indicated the influence of biomass burning on SOA formation in Xi'an in winter. In comparison, the LO-OOA resolved in Baoji and the OOA resolved in Shijiazhuang also showed minor influence from BBOA, with values located on the edge of the aged-BB region (Wang et al., 2017; Huang et al., 2019).

In order to further explain the possible pathway of OOA-BB formation and the influence of BBOA during the 2018 winter campaign, the evolution of BBOA into OOA-BB was further analyzed using a van Krevelen (VK) diagram of O/C vs. H/C ratios, which is typically employed to investigate OA evolution during field and laboratory experiments (Heald et al., 2010; Ng et al., 2011). As shown in Fig. 3c, the slope of the line that links BBOA to OOA-BB is −0.59 (between −0.5 and −1), suggesting that OOA-BB was likely formed from BBOA through the evolution of carboxylic acid moieties (Ng et al., 2011; Paglione et al., 2020). In our study, the concentration of OOA-BB increased as O_x increased, suggesting the importance of photochemical oxidation processes (Fig. 3d). The formation of OOA-BB was also enhanced under higher BBOA concentrations, confirming that OOA-BB was formed from the aging of BBOA.

The scatterplot of f_{44} vs. f_{60} for ambient data was also applied in order to further investigate OA transformation during different periods. As shown in Fig. 4a, data from Xi'an during the summer of 2019 are mainly located on the left side ($f_{60} = 0.1\,\%$–$0.5\,\%$), which is consistent with a negligible biomass burning influence and non-BBOA-influenced OA sources during the summer campaign (Duan et al., 2021). Agricultural burning was an important contributor to OA during the harvest season before 2013; however, agricultural burning during this season was banned in 2013, and BBOA sources have become a negligible contributor to OA in summertime, especially in urban city areas, in recent years (Huang et al., 2021). During the winter campaign, the data are mainly located in the lower right part of Fig. 4a, with f_{60} ranging from 0.4 % to 1.4 % on reference days, suggesting the significant influence of BBOA. The data during SIA-P1 are also mainly located in the lower right part of the figure, with f_{60} ranging from 0.7 % to 1.4 %, suggesting that BBOA also had significant influence during this period. Meanwhile, more data are located in the upper range, with higher f_{44}, than those on reference days, suggesting increased OA aging and secondary formation during SIA_P1. As for SIA_P2, more data are located on the left side of the figure (no BB influence), and the range of f_{44} is also higher compared with reference days and SIA_P1, suggesting that the BBOA influence decreased while the SOA influence and OA oxidation state increased during SIA_P2. Consistently, from reference days and SIA_P1 to SIA_P2, the contribution of BBOA decreased from 13 % and 14 % to 6 %, respectively; the OOA-BB contribution decreased from 31 % and 22 % to 16 %, respectively; and the aq-OOA contribution increased largely from 19 % and 39 % to 61 %, respectively. The scatterplot of f_{44} vs. f_{43} is also shown in Fig. 4b in order to study the evolution of SOA. The data points substantially fall into the triangle space derived by Ng et al. (2010), in which higher f_{44} and lower f_{43} are characteristics of more highly oxidized and aged aerosol, whereas lower f_{44} and higher f_{43} values represent less highly oxidized and fresh organics. From reference days to SIA_P1 and SIA_P2, OA shows evolution trends moving from the lower right to the upper left in the triangle in Fig. 4b, suggesting the increased oxidation of OA during SIA-enhanced periods (Ng et al., 2010). Consistently, the POA factors (HOA, COA, CCOA, and BBOA) are concentrated in the bottom of the triangle, OOA-BB is in an intermediate location, and aq-OOA is at the top left of the triangle with the highest oxidation state.

3.3 aq-OOA dependence on SIA and ALWC

The aq-OOA showed an obvious mass increase during the SIA-enhanced periods, and this tracked well with the ALWC increase during this winter campaign (Figs. 1, 2). In addition, the mass spectrum of aq-OOA resolved in this study was tightly correlated with that resolved in Xi'an in the summer of 2019 ($R^2 = 0.86$, Fig. S8) (Duan et al., 2021), and the time series of aq-OOA was also well correlated with $CH_2O_2^+$ ($R^2 = 0.91$), CH_3SO^+ ($R^2 = 0.89$), and $CH_3SO_2^+$ ($R^2 = 0.75$) (Fig. S8), which are the typical fragment ions of aqueous-phase processing products (Tan et al., 2009; Chhabra et al., 2010; Ge et al., 2012; Sun et al., 2016). These results suggest a dominant role of aqueous-phase processes in the formation of aq-OOA in Xi'an in winter. As shown in Fig. 5, there was a positive correlation between the concentration of aq-OOA and ALWC, with variable slopes in different RH ranges; this was likely due to the exponential increase in ALWC with RH (Wu et al., 2018). As discussed by Wu et al. (2018), simultaneously elevated RH levels and SIA concentrations result in an abundant ALWC. Condensed water also facilitates the partitioning of water-soluble polar organics into condensed phases, and this subsequently facilitate SOA formation. Consistently, a higher SIA concentration also shows a positive effect on the aq-OOA increase (Fig. 5), and a tight correlation between the concentration of aq-OOA and SIA is observed for the whole data set irrespective of the RH variation ($R^2 = 0.96$, Fig. S10).

We further compared the aqueous-phase formation of aq-OOA in Xi'an during summer 2019 and winter 2018 and discussed the specific effect of sulfate or nitrate on its formation (Fig. 6). As discussed in our previous study (Duan et al., 2021), aq-OOA was dominantly formed on fog/rain days with consistently high RH (>60 %) and ALWC conditions during summer. The concentration of aq-OOA continuously increased as RH increased from 70 % to 100 % and ALWC increased from 10 to 10–100 $\mu g\,m^{-3}$ before further increasing to >100 $\mu g\,m^{-3}$ (Fig. 6a, b). This suggests that the formation of aq-OOA is very dependent on ALWC, which might be a bulk water reaction in Xi'an in summer (Duan et al., 2021).

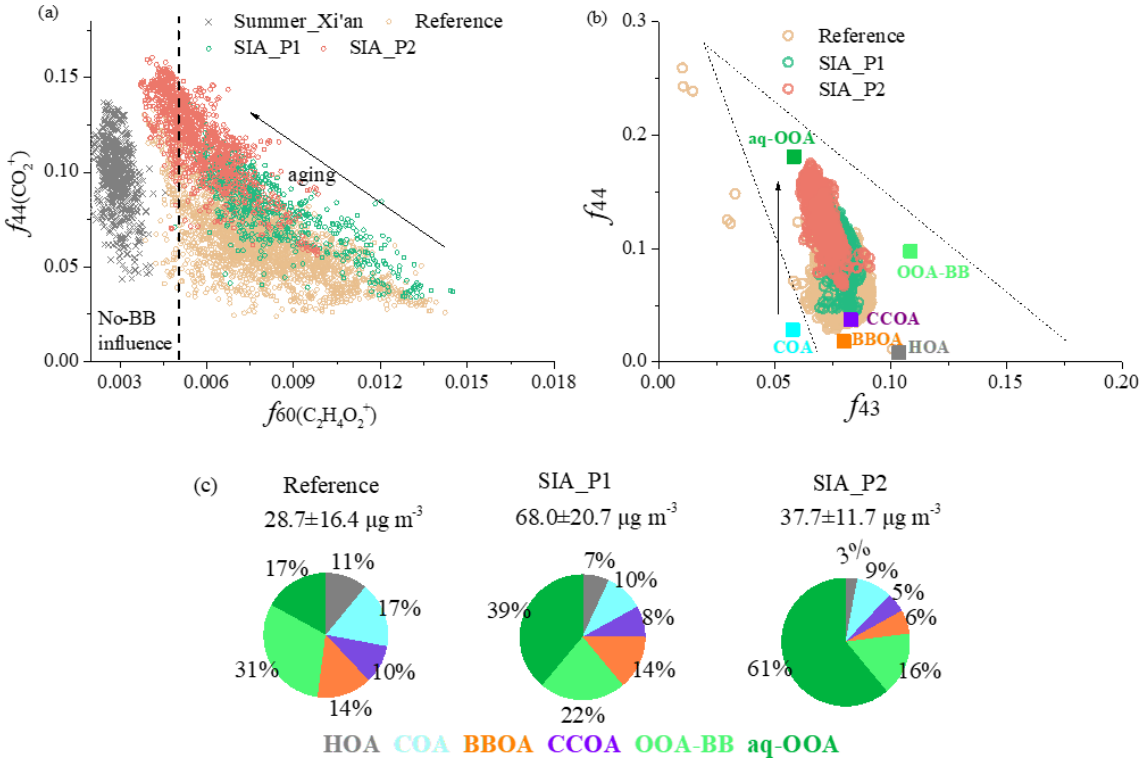

Figure 4. Panel **(a)** presents f_{44} vs. f_{60} during three periods, including reference days, SIA_P1, and SIA_P2; f_{44} vs. f_{60} in summer 2019 is also shown for comparison. Panel **(b)** shows f_{44} vs. f_{43} during these three periods; the corresponding values of the six OA factors identified in this study are also shown, and the triangle range is from Ng et al. (2010). Panel **(c)** outlines the average OA concentration and composition during these three periods.

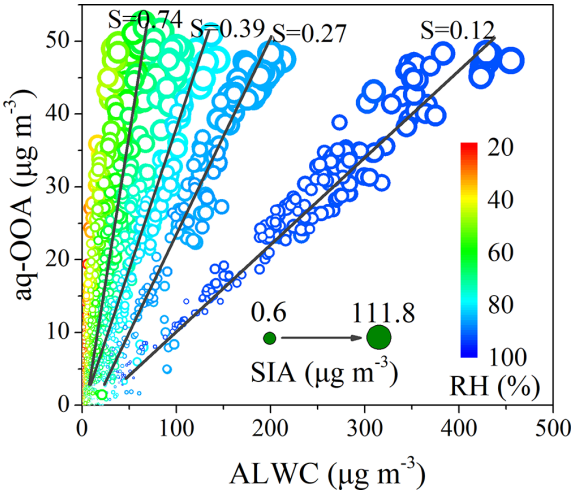

Figure 5. The effects of ALWC on the formation of aq-OOA (colored by RH), with the increase in the SIA concentration shown by the size increase in the data points. Note that "*S*" is defined as the slope between aq-OOA and ALWC in different RH ranges.

In comparison, the concentration of aq-OOA did not continuously increase as ALWC increased from 10–100 μg m^{-3} to >100 μg m^{-3}; instead, the aq-OOA concentration was much affected by the mass increase in nitrate and sulfate, with a similar aq-OOA concentration associated with a similar sulfate or nitrate concentration level under different RH ranges (Fig. 6c, d). This may suggest that aq-OOA formation is more driven by heterogeneous surface reactions in winter, as sulfate and nitrate associated with condensed water may provide the relevant media and increase the aerosol surface area, leading to an increasing heterogeneous reaction rate and modulating the formation of SOA (Wu et al., 2018). Nitrate displayed a more positive effect on aq-OOA formation than sulfate in summer, as sulfate showed a weaker correlation ($R^2 = 0.44$) with aq-OOA than that of nitrate ($R^2 = 0.98$) (Fig. S11). In contrast to aq-OOA in summer, which was mainly formed when RH >60 %, the formation of aq-OOA in winter was frequently observed when RH >40 % (Fig. 6c, d). This may be related to the much higher nitrate contribution during winter which reduces the deliquesce RH of the aerosol mixture and provides liquid-phase conditions for aq-OOA formation at even lower RH (Xue et al., 2014; Wu et al., 2018). When the ALWC was higher than 10 μg m^{-3}, aq-OOA was formed efficiently, and both nitrate and sulfate displayed positive ef-

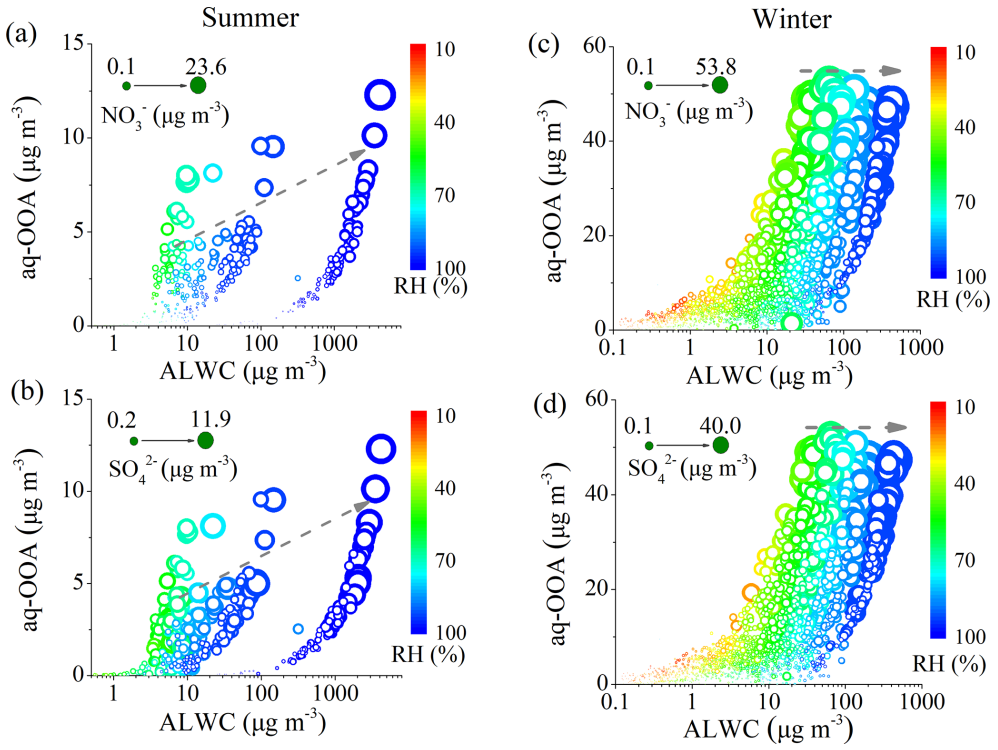

Figure 6. Correlations between ALWC and aq-OOA in Xi'an (colored by RH) during summer **(a, b)** and winter **(c, d)**. The effects of nitrate **(a, c)** and sulfate **(b, d)** are also shown; the increase in the sulfate or nitrate concentration is shown by the size increase in the data points. The summer data were taken from Duan et al. (2021), and the horizontal axes in both summer and winter are shown in exponential format for comparison.

fects on the aq-OOA increase. Moreover, as shown in Fig. 5, the correlation slope (S) between aq-OOA and ALWC decreases from 0.74 for RH <70 % to 0.12 for RH>90 %, which means that aq-OOA did not show a increase that was proportional to the exponential increase in ALWC with high RH, and the slope decreased. In comparison, a similar aq-OOA concentration was associated with similar SIA concentration levels under different RH ranges. These results suggest that SIA, compared with RH and ALWC, may play a much more important role in the formation of aq-OOA in Xi'an in winter.

3.4 The van Krevelen analysis: the importance of aqueous-phase processes

The VK diagram, displaying the variation in O/C vs. H/C (Hu et al., 2013), was further used to probe OA oxidation reaction mechanisms in our study. As shown in Fig. 7a, data with a higher O/C ratio and lower H/C ratio, located in the bottom right corner, are usually related to a higher SIA concentration, and a higher ALWC also facilitated the increase in the O/C ratio, suggesting the positive effects of SIA and aqueous-phase processes on OA oxidation enhancement during winter in Xi'an. The slope and intercept of the VK diagram for OA during different periods are further displayed in Fig. 7b. More data are located in the bottom right corner (higher O/C ratio) during SIA-enhanced periods than those during reference days, especially in SIA_P2 which had a much higher fraction of aq-OOA. Meanwhile, the slope of the correlation between H/C and O/C during SIA-enhanced periods is also more gentle than that for reference days; note the change from −0.49 for reference days to −0.39 during SIA_P1 and −0.33 during SIA_P2. This suggests the addition of carboxylic acid groups with fragmentation (slope = −0.5) dominated OA aging on reference days, and the variation in the slope might suggest the transformation of OA from reference days to SIA-enhanced periods, which likely reflects OA evolution due to the addition of alcohol or peroxide groups (slope ≈ 0) (Heald et al., 2010; Chen et al., 2015).

4 Conclusion

The NR-$PM_{2.5}$ chemical composition and OA sources were characterized in Xi'an during the residential heating season of 2018. The average mass concentration of NR-$PM_{2.5}$ was $68.0 \pm 42.8\,\mu g\,m^{-3}$, which is higher than that in Xi'an during the summer of 2019 but much lower than that during the winter of 2013. Six OA sources, including HOA, COA, CCOA, BBOA, OOA-BB, and aq-OOA, were resolved, and SOA was

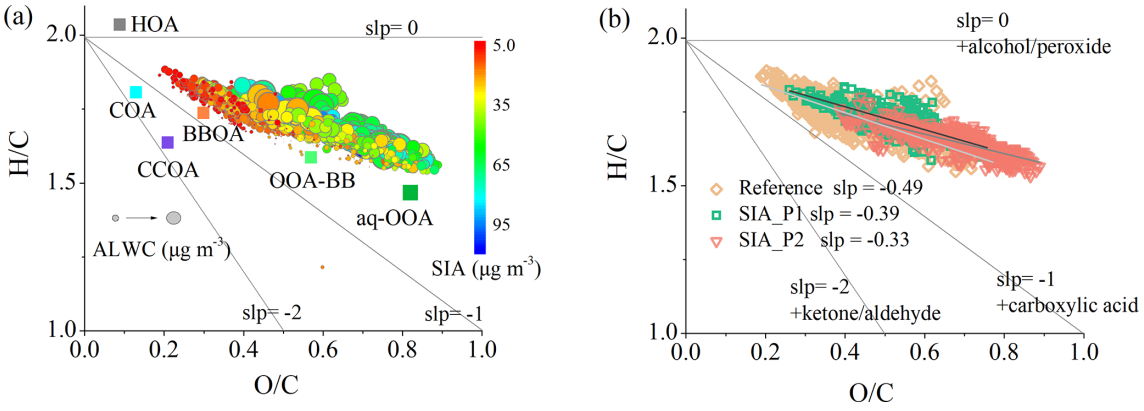

Figure 7. The VK diagram of H/C vs. O/C for the entire winter observation period **(a)** as well as for different periods, including reference days, SIA_P1, and SIA_P2 **(b)**. The scatterplots of H/C vs. O/C are colored by the mass concentration of SIA, and the size of the data points is proportional to the ALWC concentration in panel **(a)**.

found to contribute to total OA mass to a much larger extent (58 %) than POA (42 %). Further formation mechanism analysis showed that OOA-BB was mainly formed from the photochemical oxidation and aging of BBOA and that formation was more favorable on reference days with a higher BBOA concentration. In comparison, aq-OOA was dominated by aqueous-phase processes, which showed an obvious mass increase during SIA-enhanced periods, and tracked well with the ALWC. From reference days to SIA-enhanced periods (which usually related to haze pollution), aq-OOA increased obviously, with the aq-OOA concentration (fraction) increasing from $4.9 \pm 3.7\,\mu g\,m^{-3}$ (17 %) during reference days to $26.2 \pm 14.6\,\mu g\,m^{-3}$ (39 %) during SIA_P1 and to $22.7 \pm 10.7\,\mu g\,m^{-3}$ (61 %) during SIA_P2, suggesting the critical role of aqueous-phase processes in haze pollution in Xi'an during winter. Consistently, the O/C ratio of bulk OA increased from 0.41 during reference days to 0.52 during SIA_P1 and to 0.67 during SIA_P2, with the VK slope of H/C vs. O/C changing from −0.49 to −0.39 during SIA_P1 and to −0.33 during SIA_P2. This suggests that the increased aq-OOA contribution during SIA-enhanced periods likely reflects OA evolution due to the addition of alcohol or peroxide groups.

Data availability. The key data sets are archived at the East Asian Paleoenvironmental Science Database, National Earth System Science Data Center, National Science and Technology Infrastructure of China: https://doi.org/10.12262/IEECAS.EAPSD2022004 (Duan et al., 2022). For further information, please contact the corresponding author (rujin.huang@ieecas.cn).

Supplement. The supplement related to this article is available online at: https://doi.org/10.5194/acp-22-10139-2022-supplement.

Author contributions. RJH designed the study. JD, YG, CL, and HZ conducted the field observations. Data analysis and source apportionment were done by JD and RJH, with help from WX, QL, and YY. JD and RJH wrote the manuscript. JD and RJH interpreted data and prepared display items. JO, DC, TH, and CO'D all commented on and discussed the manuscript.

Competing interests. The contact author has declared that none of the authors has any competing interests.

Disclaimer. Publisher's note: Copernicus Publications remains neutral with regard to jurisdictional claims in published maps and institutional affiliations.

Acknowledgements. The authors acknowledge support from the National Natural Science Foundation of China (grant no. 41925015), the Strategic Priority Research Program of Chinese Academy of Sciences (grant no. XDB40000000), the Chinese Academy of Sciences (grant no. ZDBS-LY-DQC001), and the Cross Innovative Team fund from the State Key Laboratory of Loess and Quaternary Geology (grant no. SKLLQGTD1801).

Financial support. This research has been supported by the National Natural Science Foundation of China (grant no. 41925015), the Strategic Priority Research Program of Chinese Academy of Sciences (grant no. XDB40000000), the Chinese Academy of Sciences (grant no. ZDBS-LY-DQC001), and the Cross Innovative Team fund from the State Key Laboratory of Loess and Quaternary Geology (grant no. SKLLQGTD1801).

Review statement. This paper was edited by Barbara Ervens and reviewed by two anonymous referees.

References

Alfarra, M. R., Prevot, A. S. H., Szidat, S., Sandradewi, J., Weimer, S., Lanz, V. A., Schreiber, D., Mohr, M., and Baltensperger, U.: Identification of the mass spectral signature of organic aerosols from wood burning emissions, Environ. Sci. Technol., 41, 5770–5777, https://doi.org/10.1021/es062289b, 2007.

An, Z. S., Huang, R.-J., Zhang, R. Y., Tie, X. X., Li, G. H., Cao, J. J., Zhou, W. J., Shi, Z. G., Han, Y. M., Gu, Z. L., and Ji, Y. M.: Severe haze in northern China: A synergy of anthropogenic emissions and atmospheric processes, Proc. Natl. Acad. Sci., 116, 8657–8666, https://doi.org/10.1073/pnas.1900125116, 2019.

Canagaratna, M. R., Jimenez, J. L., Kroll, J. H., Chen, Q., Kessler, S. H., Massoli, P., Hildebrandt Ruiz, L., Fortner, E., Williams, L. R., Wilson, K. R., Surratt, J. D., Donahue, N. M., Jayne, J. T., and Worsnop, D. R.: Elemental ratio measurements of organic compounds using aerosol mass spectrometry: characterization, improved calibration, and implications, Atmos. Chem. Phys., 15, 253–272, https://doi.org/10.5194/acp-15-253-2015, 2015.

Canonaco, F., Crippa, M., Slowik, J. G., Baltensperger, U., and Prévôt, A. S. H.: SoFi, an IGOR-based interface for the efficient use of the generalized multilinear engine (ME-2) for the source apportionment: ME-2 application to aerosol mass spectrometer data, Atmos. Meas. Tech., 6, 3649–3661, https://doi.org/10.5194/amt-6-3649-2013, 2013.

Chang, Y., Huang, R.-J., Ge, X., Huang, X., Hu, J., Duan, Y., Zou, Z., Liu, X., and Lehmannet, M.F.: Puzzling haze events in China during the coronavirus (COVID-19) shutdown, Geophys. Res. Lett., 47, e2020GL088533, https://doi.org/10.1029/2020GL088533, 2020.

Chen, Q., Heald, C. L., Jimenez, J. L., Canagaratna, M. R., Zhang, Q., He, L.-Y., Huang, X.-F., Campuzano-Jost, P., Palm, B. B., Poulain, L., Kuwata, M., Martin, S. T., Abbatt, J. P. D., Lee, A. K. Y., and Liggio, J.: Elemental Composition of Organic Aerosol: The Gap Between Ambient and Laboratory Measurements, Geophys. Res. Lett., 42, 4182–4189, https://doi.org/10.1002/2015GL063693, 2015.

Chhabra, P. S., Flagan, R. C., and Seinfeld, J. H.: Elemental analysis of chamber organic aerosol using an aerodyne high-resolution aerosol mass spectrometer, Atmos. Chem. Phys., 10, 4111–4131, https://doi.org/10.5194/acp-10-4111-2010, 2010.

Cubison, M. J., Ortega, A. M., Hayes, P. L., Farmer, D. K., Day, D., Lechner, M. J., Brune, W. H., Apel, E., Diskin, G. S., Fisher, J. A., Fuelberg, H. E., Hecobian, A., Knapp, D. J., Mikoviny, T., Riemer, D., Sachse, G. W., Sessions, W., Weber, R. J., Weinheimer, A. J., Wisthaler, A., and Jimenez, J. L.: Effects of aging on organic aerosol from open biomass burning smoke in aircraft and laboratory studies, Atmos. Chem. Phys., 11, 12049–12064, https://doi.org/10.5194/acp-11-12049-2011, 2011.

DeCarlo, P. F., Kimmel, J. R., Trimborn, A., Northway, M. J., Jayne, J. T., Aiken, A. C., Gonin, M., Fuhrer, K., Horvath, T., Docherty, K. S., Worsnop, D. R., and Jimenez, J. L.: Field-deployable, high-resolution, time-of-flight aerosol mass spectrometer, Anal. Chem., 78, 8281–8289, https://doi.org/10.1021/ac061249n, 2006.

Duan, J., Huang, R. J., Gu, Y., Lin, C., Zhong, H., Wang, Y., Yuan, W., Ni, H.Y., Yang, L., Chen, Y., Worsnop, D.R., and O'Dowd, C.: The formation and evolution of secondary organic aerosol during summer in Xi'an: Aqueous phase processing in fog-rain days, Sci. Total. Environ., 756, 144077, https://doi.org/10.1016/j.scitotenv.2020.144077, 2021.

Duan, J., Huang, R.-J., Gu, Y., Lin, C., Zhong, H., Xu, W., Liu, Q., You, Y., Ovadnevaite, J., Ceburnis, D., Hoffmann, T., and O'Dowd, C.: Data for "Measurement report: Large contribution of biomass burning and aqueous-phase processes to the wintertime secondary organic aerosol formation in Xi'an, Northwest China", IEECAS.EAPSD [data set], https://doi.org/10.12262/IEECAS.EAPSD2022004, 2022.

Elser, M., Huang, R.-J., Wolf, R., Slowik, J. G., Wang, Q., Canonaco, F., Li, G., Bozzetti, C., Daellenbach, K. R., Huang, Y., Zhang, R., Li, Z., Cao, J., Baltensperger, U., El-Haddad, I., and Prévôt, A. S. H.: New insights into $PM_{2.5}$ chemical composition and sources in two major cities in China during extreme haze events using aerosol mass spectrometry, Atmos. Chem. Phys., 16, 3207–3225, https://doi.org/10.5194/acp-16-3207-2016, 2016.

Fountoukis, C. and Nenes, A.: ISORROPIA II: a computationally efficient thermodynamic equilibrium model for $K^+-Ca^{2+}-Mg^{2+}-NH_4^+-Na^+-SO_4^{2-}-NO_3^--Cl^--H_2O$ aerosols, Atmos. Chem. Phys., 7, 4639–4659, https://doi.org/10.5194/acp-7-4639-2007, 2007.

Ge, X., Setyan, A., Sun, Y., and Zhang, Q.: Primary and secondary organic aerosols in Fresno, California during wintertime: Results from high resolution aerosol mass spectrometry, J. Geophys. Res., 117, D19301, https://doi.org/10.1029/2012jd018026, 2012.

Gilardoni, S., Massoli, P., Paglione, M., Giulianelli, L., Carbone, C., Rinaldi, M., Decesari, S., Sandrini, S., Costabile, F., Gobbi, G. P., Pietrogrande, M. C., Visentin, M., Scotto, F., Fuzzi, S., and Facchini, M. C.: Direct observation of aqueous secondary organic aerosol from biomass burning emissions, P. Natl. Acad. Sci. USA, 113, 10013–10018, https://doi.org/10.1073/pnas.1602212113, 2016.

Guo, S., Hu, M., Zamora, M. L., Peng, J., Shang, D., Zheng, J., Du, Z., Wu, Z., Shao, M., Zeng, L., Molina, M. J., and Zhang, R.: Elucidating severe urban haze formation in China, Proc. Natl. Acad. Sci., 111, 17373–17378, https://doi.org/10.1073/pnas.1419604111, 2014.

Heald, C. L., Kroll, J. H., Jimenez, J. L., Docherty, K. S., DeCarlo, P. F., Aiken, A. C., Chen, Q., Martin, S. T., Farmer, D. K., and Artaxo, P.: A simplified description of the evolution of organic aerosol composition in the atmosphere, Geophys. Res. Lett., 37, L08803, https://doi.org/10.1029/2010GL042737, 2010.

Hu, W. W., Hu, M., Yuan, B., Jimenez, J. L., Tang, Q., Peng, J. F., Hu, W., Shao, M., Wang, M., Zeng, L. M., Wu, Y. S., Gong, Z. H., Huang, X. F., and He, L. Y.: Insights on organic aerosol aging and the influence of coal combustion at a regional receptor site of central eastern China, Atmos. Chem. Phys., 13, 10095–10112, https://doi.org/10.5194/acp-13-10095-2013, 2013.

Hu, W. W., Hu, M., Hu, W., Jimenez, J. L., Yuan, B., Chen, W., Wang, M., Wu, Y., Chen, C., Wang, Z., Peng, J., Zeng, L., and Shao, M.: Chemical composition, sources, and aging process of submicron aerosols in Beijing: Contrast between summer and winter, J. Geophys. Res.-Atmos., 121, 1955–1977, https://doi.org/10.1002/2015JD024020, 2016.

Huang, L., Zhu, Y., Wang, Q., Zhu, A., Liu, Z., Wang, Y., Allen, D. T., and Li, L.: Assessment of the effects of straw burning bans in China: Emissions, air qual-

ity, and health impacts, Sci. Total. Environ., 789, 147935, https://doi.org/10.1016/j.scitotenv.2021.147935, 2021.

Huang, R.-J., Zhang, Y. L., Bozzetti, C., Ho, K.-F., Cao, J. J., Han, Y. M., Daellenbach, K. R., Slowik, J. G., Platt, S. M., Canonaco, F., Zotter, P., Wolf, R., Pieber, S. M., Bruns, E. A., Crippa, M., Ciarelli, G., Piazzalunga, A., Schwikowski, M., Abbaszade, G., Schnelle-Kreis, J., Zimmermann, R., An, Z., Szidat, S., Baltensperger, U., Haddad, I. E., and Prévôt, A. S. H.: High secondary aerosol contribution to particulate pollution during haze events in China, Nature, 514, 218–222, https://doi.org/10.1038/nature13774, 2014.

Huang, R.-J., Wang, Y., Cao, J., Lin, C., Duan, J., Chen, Q., Li, Y., Gu, Y., Yan, J., Xu, W., Fröhlich, R., Canonaco, F., Bozzetti, C., Ovadnevaite, J., Ceburnis, D., Canagaratna, M. R., Jayne, J., Worsnop, D. R., El-Haddad, I., Prévôt, A. S. H., and O'Dowd, C. D.: Primary emissions versus secondary formation of fine particulate matter in the most polluted city (Shijiazhuang) in North China, Atmos. Chem. Phys., 19, 2283–2298, https://doi.org/10.5194/acp-19-2283-2019, 2019.

Huang, R.-J., He, Y., Duan, J., Li, Y., Chen, Q., Zheng, Y., Chen, Y., Hu, W., Lin, C., Ni, H., Dai, W., Cao, J., Wu, Y., Zhang, R., Xu, W., Ovadnevaite, J., Ceburnis, D., Hoffmann, T., and O'Dowd, C. D.: Contrasting sources and processes of particulate species in haze days with low and high relative humidity in wintertime Beijing, Atmos. Chem. Phys., 20, 9101–9114, https://doi.org/10.5194/acp-20-9101-2020, 2020.

Ji, Y., Qin, X., Wang, B., Xu, J., Shen, J., Chen, J., Huang, K., Deng, C., Yan, R., Xu, K., and Zhang, T.: Counteractive effects of regional transport and emission control on the formation of fine particles: a case study during the Hangzhou G20 summit, Atmos. Chem. Phys., 18, 13581–13600, https://doi.org/10.5194/acp-18-13581-2018, 2018.

Jimenez, J. L., Jayne, J. T., Shi, Q., Kolb, C. E., Worsnop, D. R., Yourshaw, I., Seinfeld, J. H., Flagan, R. C., Zhang, X., Smith, K. A., Morris, J. W., and Davidovits, P.: Ambient aerosol sampling with an Aerosol Mass Spectrometer, J. Geophys. Res.-Atmos., 108, 8425, https://doi.org/10.1029/2001JD001213, 2003.

Jimenez, J. L., Canagaratna, M. R., Donahue, N. M., Prevot, A. S. H., Zhang, Q., Kroll, J. H., DeCarlo, P. F., Allan, J. D., Coe, H., Ng, N. L., Aiken, A. C., Docherty, K. S., Ulbrich, I. M., Grieshop, A. P., Robinson, A. L., Duplissy, J., Smith, J. D., Wilson, K. R., Lanz, V. A., Hueglin, C., Sun, Y. L., Tian, J., Laaksonen, A., Raatikainen, T., Rautiainen, J., Vaattovaara, P., Ehn, M., Kulmala, M., Tomlinson, J. M., Collins, D. R., Cubison, M. J., Dunlea, J., Huffman, J. A., Onasch, T. B., Alfarra, M. R., Williams, P. I., Bower, K., Kondo, Y., Schneider, J., Drewnick, F., Borrmann, S., Weimer, S., Demerjian, K., Salcedo, D., Cottrell, L., Griffin, R., Takami, A., Miyoshi, T., Hatakeyama, S., Shimono, A., Sun, J. Y., Zhang, Y. M., Dzepina, K., Kimmel, J. R., Sueper, D., Jayne, J. T., Herndon, S. C., Trimborn, A. M., Williams, L. R., Wood, E. C., Middlebrook, A. M., Kolb, C. E., Baltensperger, U., and Worsnop, D. R.: Evolution of Organic Aerosols in the Atmosphere, Science, 326, 1525–1529, https://doi.org/10.1126/science.1180353, 2009.

Kuang, Y., He, Y., Xu, W. Y., Yuan, B., Zhang, G., Ma, Z. Q., Wu, C. H., Wang, C. M., Wang, S. H., Zhang, S. Y., Tao, J. C., Ma, N., Su, H., Cheng, Y. F., Shao, M., and Sun, Y. L.: Photochemical aqueous-phase reactions induce rapid daytime formation of oxygenated organic aerosol on the North China Plain, Environ. Sci. Technol., 54, 3849–3860, https://doi.org/10.1021/acs.est.9b06836, 2020.

Lelieveld, J., Evans, J. S., Fnais, M., Giannadaki, D., and Pozzer, A.: The contribution of outdoor air pollution sources to premature mortality on a global scale, Nature, 525, 367–371, https://doi.org/10.1038/nature15371, 2015.

Li, J., Han, Z., Sun, Y., Li, J., and Liang, L.: Chemical formation pathways of secondary organic aerosols in the Beijing-Tianjin-Hebei region in wintertime, Atmos. Environ., 244, 117996, https://doi.org/10.1016/j.atmosenv.2020.117996, 2021.

Li, J., Deng, S., Li, G., Lu, Z., Song, H., Gao, J., Sun, Z., and Xu, K.: VOCs characteristics and their ozone and SOA formation potentials in autumn and winter at Weinan, China, Environ. Res., 203, 111821, https://doi.org/10.1016/j.envres.2021.111821, 2022a.

Li, X., Sun, N., Jin, Q., Zhao, Z., Wang, L., Wang, Q., Gu, X., Li, Y., and Liu, X.: Light absorption properties of black and brown carbon in winter over the North China Plain: Impacts of regional biomass burning, Atmos. Environ., 278, 119100, https://doi.org/10.1016/j.atmosenv.2022.119100, 2022b.

Li, Y. J., Sun, Y., Zhang, Q., Li, X., Li, M., Zhou, Z., and Chan, C. K.: Real-time chemical characterization of atmospheric particulate matter in China: a review, Atmos. Environ., 158, 270–304, https://doi.org/10.1016/j.atmosenv.2017.02.027, 2017.

Liu, Z., Wang, Y., Gu, D., Zhao, C., Huey, L. G., Stickel, R., Liao, J., Shao, M., Zhu, T., Zeng, L., Liu, S.-C., Chang, C.-C., Amoroso, A., and Costabile, F.: Evidence of reactive aromatics as a major source of peroxy acetyl nitrate over China, Environ. Sci. Technol., 44, 7017–7022, https://doi.org/10.1021/es1007966, 2010.

Lv, S., Wang, F., Wu, C., Chen, Y., Liu, S., Zhang, S., Li, D., Du, W., Zhang, F., Wang, H., Huang, C., Fu, Q., Duan, Y., and Wang, G.: Gas-to-Aerosol Phase Partitioning of Atmospheric Water-Soluble Organic Compounds at a Rural Site in China: An Enhancing Effect of NH_3 on SOA Formation, Environ. Sci. Technol., 56, 3915–3924, https://doi.org/10.1021/acs.est.1c06855, 2022.

Middlebrook, A. M., Bahreini, R., Jimenez, J. L., and Canagaratna, M. R.: Evaluation of composition-dependent collection efficiencies for the Aerodyne Aerosol Mass Spectrometer using field data, Aerosol Sci. Tech., 46, 258–271, https://doi.org/10.1080/02786826.2011.620041, 2012.

Ng, N. L., Canagaratna, M. R., Zhang, Q., Jimenez, J. L., Tian, J., Ulbrich, I. M., Kroll, J. H., Docherty, K. S., Chhabra, P. S., Bahreini, R., Murphy, S. M., Seinfeld, J. H., Hildebrandt, L., Donahue, N. M., DeCarlo, P. F., Lanz, V. A., Prévôt, A. S. H., Dinar, E., Rudich, Y., and Worsnop, D. R.: Organic aerosol components observed in Northern Hemispheric datasets from Aerosol Mass Spectrometry, Atmos. Chem. Phys., 10, 4625–4641, https://doi.org/10.5194/acp-10-4625-2010, 2010.

Ng, N. L., Canagaratna, M. R., Jimenez, J. L., Chhabra, P. S., Seinfeld, J. H., and Worsnop, D. R.: Changes in organic aerosol composition with aging inferred from aerosol mass spectra, Atmos. Chem. Phys., 11, 6465–6474, https://doi.org/10.5194/acp-11-6465-2011, 2011.

Onasch, T. B., Trimborn, A., Fortner, E. C., Jayne, J. T., Kok, G. L., Williams, L. R., Davidovits, P., and Worsnop, D. R.: Soot particle aerosol mass spectrometer: development, validation, and initial application, Aerosol. Sci. Tech., 46, 804–817, https://doi.org/10.1080/02786826.2012.663948, 2012.

Paatero, P.: The multilinear engine: a table-driven, least squares program for solving multilinear problems, including the n-way parallel factor analysis model, J. Comput. Graph. Stat., 8, 854–888, https://doi.org/10.1080/10618600.1999.10474853, 1999.

Paglione, M., Gilardoni, S., Rinaldi, M., Decesari, S., Zanca, N., Sandrini, S., Giulianelli, L., Bacco, D., Ferrari, S., Poluzzi, V., Scotto, F., Trentini, A., Poulain, L., Herrmann, H., Wiedensohler, A., Canonaco, F., Prévôt, A. S. H., Massoli, P., Carbone, C., Facchini, M. C., and Fuzzi, S.: The impact of biomass burning and aqueous-phase processing on air quality: a multi-year source apportionment study in the Po Valley, Italy, Atmos. Chem. Phys., 20, 1233–1254, https://doi.org/10.5194/acp-20-1233-2020, 2020.

Peng, J., Hu, M., Guo, S., Du, Z., Zheng, J., Shang, D., Levy Zamora, M., Zeng, L., Shao, M., Wu, Y., Zheng, J., Wang, Y., Glen, C. R., Collins, D. R., Molina, M. J., and Zhang, R.: Markedly enhanced absorption and direct radiative forcing of black carbon under polluted urban environments, Proc. Natl. Acad. Sci., 113, 4266–4271, https://doi.org/10.1073/pnas.1602310113, 2016.

Shrivastava, M., Cappa, C. D., Fan, J. W., Goldstein, A. H., Guenther, A. B., Jimenez, J. L., Kuang, C., Laskin, A., Martin, S. T., Ng, N. L., Petaja, T., Pierce, J. R., Rasch, P. J., Roldin, P., Seinfeld, J. H., Shilling, J., Smith, J. N., Thornton, J. A., Volkamer, R., Wang, J., Worsnop, D. R., Zaveri, R. A., Zelenyuk, A., and Zhang, Q.: Recent advances in understanding secondary organic aerosol: Implications for global climate forcing, Rev. Geophys., 55, 509–559, https://doi.org/10.1002/2016RG000540, 2017.

Sun, Y., Wang, Z. F., Fu, P. Q., Yang, T., Jiang, Q., Dong, H. B., Li, J., and Jia, J. J.: Aerosol composition, sources and processes during wintertime in Beijing, China, Atmos. Chem. Phys., 13, 4577–4592, https://doi.org/10.5194/acp-13-4577-2013, 2013.

Sun, Y., Jiang, Q., Wang, Z., Fu, P., Li, J., Yang, T., and Yin, Y.: Investigation of the sources and evolution processes of severe haze pollution in Beijing in January 2013, J. Geophys. Res.-Atmos., 119, 4380–4398, https://doi.org/10.1002/2014JD021641, 2014.

Sun, Y., Wang, Z. F., Du, W., Zhang, Q., Wang, Q. Q., Fu, P. Q., Pan, X. L., Li, J., Jayne, J., and Worsnop, D. R.: Long-term real-time measurements of aerosol particle composition in Beijing, China: seasonal variations, meteorological effects, and source analysis, Atmos. Chem. Phys., 15, 10149–10165, https://doi.org/10.5194/acp-15-10149-2015, 2015.

Sun, Y., Du, W., Fu, P., Wang, Q., Li, J., Ge, X., Zhang, Q., Zhu, C., Ren, L., Xu, W., Zhao, J., Han, T., Worsnop, D. R., and Wang, Z.: Primary and secondary aerosols in Beijing in winter: sources, variations and processes, Atmos. Chem. Phys., 16, 8309–8329, https://doi.org/10.5194/acp-16-8309-2016, 2016.

Sun, Y., Xu, W., Zhang, Q., Jiang, Q., Canonaco, F., Prévôt, A. S. H., Fu, P., Li, J., Jayne, J., Worsnop, D. R., and Wang, Z.: Source apportionment of organic aerosol from 2-year highly time-resolved measurements by an aerosol chemical speciation monitor in Beijing, China, Atmos. Chem. Phys., 18, 8469–8489, https://doi.org/10.5194/acp-18-8469-2018, 2018.

Tan, Y., Perri, M. J., Seitzinger, S. P., and Turpin, B. J.: Effects of Precursor Concentration and Acidic Sulfate in Aqueous Glyoxal-OH Radical Oxidation and Implications for Secondary Organic Aerosol, Environ. Sci. Technol., 43, 8105–8112, https://doi.org/10.1021/es901742f, 2009.

Tong, Z., Yang, B., Hopke, P. K., and Zhang, K. M.: Microenvironmental air quality impact of a commercial-scale biomass heating system, Environ. Pollut., 220, 1112–1120, https://doi.org/10.1016/j.envpol.2016.11.025, 2017.

Wan, J., Qin, C., Wang, Q., Xiao, Y., Niu, R., Li, X., and Su, J.: A Brief Overview of the 13th Five-Year Plan for the Protection of Ecological Environment, in: Environmental Strategy and Planning in China, edited by: Wang, J., Wang, X., and Wan, J., Springer, Singapore, 57–85, https://doi.org/10.1007/978-981-16-6909-5_3, 2022.

Wang, Y. C., Huang, R.-J., Ni, H. Y., Chen, Y., Wang, Q. Y., Li, G. H., Tie, X. X., Shen, Z. X., Huang, Y., Liu, S. X., Dong, W. M., Xue, P., Fröhlich, R., Canonaco, F., Elser, M., Daellenbach, K. R., Bozzetti, C., Haddad, E. I., and Cao, J. J.: Chemical composition, sources and secondary processes of aerosols in Baoji city of northwest China, Atmos. Environ., 158, 128–137, https://doi.org/10.1016/j.atmosenv.2017.03.026, 2017.

Wu, Z., Wang, Y., Tan, T., Zhu, Y., Li, M., Shang, D., Wang, H., Lu, K., Guo, S., Zeng, L., and Zhang, Y.: Aerosol liquid water driven by anthropogenic inorganic salts: implying its key role in haze formation over the North China Plain, Environ. Sci. Tech. Lett., 5, 160–166, https://doi.org/10.1021/acs.estlett.8b00021, 2018.

Xiao, H. W., Wu, J. F., Luo, L., Liu, C., Xie, Y. J., and Xiao, H. Y.: Enhanced biomass burning as a source of aerosol ammonium over cities in central China in autumn, Environ. Pollut., 266, 115278, https://doi.org/10.1016/j.envpol.2020.115278, 2020.

Xu, J., Zhang, Q., Chen, M., Ge, X., Ren, J., and Qin, D.: Chemical composition, sources, and processes of urban aerosols during summertime in northwest China: insights from high-resolution aerosol mass spectrometry, Atmos. Chem. Phys., 14, 12593–12611, https://doi.org/10.5194/acp-14-12593-2014, 2014.

Xu, J., Shi, J., Zhang, Q., Ge, X., Canonaco, F., Prévôt, A. S. H., Vonwiller, M., Szidat, S., Ge, J., Ma, J., An, Y., Kang, S., and Qin, D.: Wintertime organic and inorganic aerosols in Lanzhou, China: sources, processes, and comparison with the results during summer, Atmos. Chem. Phys., 16, 14937–14957, https://doi.org/10.5194/acp-16-14937-2016, 2016.

Xu, W. Q., Han, T. T., Du, W., Wang, Q. Q., Chen, C., Zhao, J., Zhang, Y. J., Li, J., Fu, P. Q., Wang, Z. F., Worsnop, D. R., and Sun, Y. L.: Effects of Aqueous-Phase and Photochemical Processing on Secondary Organic Aerosol Formation and Evolution in Beijing, China, Environ. Sci. Technol., 51, 762–770, https://doi.org/10.1021/acs.est.6b04498, 2017.

Xu, W., Sun, Y., Wang, Q., Zhao, J., Wang, J., Ge, X., Xie, C., Zhou, W., Du, W., Li, J., Fu, P., Wang, Z., Worsnop, D. R., and Coe, H.: Changes in aerosol chemistry from 2014 to 2016 in winter in Beijing: Insights from high-resolution aerosol mass spectrometry, J. Geophys. Res.-Atmos., 124, 1132–1147, https://doi.org/10.1029/2018JD029245, 2019.

Xue, J., Griffith, S. M., Yu, X., Lau, A. K. H., and Yu, J. Z.: Effect of nitrate and sulfate relative abundance in $PM_{2.5}$ on liquid water content explored through half-hourly observations of inorganic soluble aerosols at a polluted receptor site, Atmos. Environ., 99, 24–31, https://doi.org/10.1016/j.atmosenv.2014.09.049, 2014.

Yuan, W., Huang, R. J., Yang, L., Ni, H., Wang, T., Cao, W., Duan, J., Guo, J., Huang, H., and Hoffmann, T.: Concentrations, optical properties and sources of humic-like substances (HULIS) in fine particulate matter in

Xi'an, Northwest China, Sci. Total. Environ., 789, 147902, https://doi.org/10.1016/j.scitotenv.2021.147902, 2021.

Zhang, H., Chen, C., Yan, W., Wu, N., Bo, Y., Zhang, Q., and He, K.: Characteristics and sources of non-methane VOCs and their roles in SOA formation during autumn in a central Chinese city, Sci. Total. Environ., 782, 146802, https://doi.org/10.1016/j.scitotenv.2021.146802, 2021a.

Zhang, T., Shen, Z., Zhang, L., Tang, Z., Zhang, Q., Chen, Q., Lei, Y., Zeng, Y., Xu, H., and Cao, J.: $PM_{2.5}$ Humic-like substances over Xi'an, China: Optical properties, chemical functional group, and source identification, Atmos. Res., 234, 104784, https://doi.org/10.1016/j.atmosres.2019.104784, 2020.

Zhang, T., Shen, Z., Zeng, Y., Cheng, C., Wang, D., Zhang, Q., Lei, Y., Zhang, Y., Sun, J., Xu, H., Ho, S. S. H., and Cao, J.: Light absorption properties and molecular profiles of HULIS in $PM_{2.5}$ emitted from biomass burning in traditional "Heated Kang" in Northwest China, Sci. Total. Environ., 776, 146014, https://doi.org/10.1016/j.scitotenv.2021.146014, 2021b.

Zhong, H., Huang, R.-J., Duan, J., Lin, C., Gu, Y., Wang, Y., Li, Y. J., Zheng, Y., Chen, Q., Chen, Y., Dai, W. T., Ni, H. Y., Cao, J. J., Worsnop, D. R., Xu, W., Ovadnevaite, J., Ceburnis, D., and O'Dowd, C. D.: Seasonal variations in the sources of organic aerosol in Xi'an, Northwest China: The importance of biomass burning and secondary formation, Sci. Total. Environ., 737, 139666, https://doi.org/10.1016/j.scitotenv.2020.139666, 2020.